Journal of Solar Energy Research (JSER)

Journal homepage: www.jser.ut.ac.ir

# Computational Analysis of Radial Turbine Design and Performance for Renewable Power Generation in Solar Chimney

Youcef Bouzida[a,b *], Abdelmadjid Chehhat[a,b], Mohamed Si-Ameur[b], Toufik Arrif[c]

[a]*Department of Mechanical Engineering, University of Abbas Laghrour Khenchela, 40004 Khenchela, Algeria*
[b]*Laboratory of Studies of Industrial Energy Systems LESEI, Faculty of Technology, University of Batna 2, 05000 Batna, Algeria*
[c]*Unité de Recherche Appliquée en Energies Renouvelables, URAER, Centre de Développement des Energies Renouvelables, CDER, Ghardaïa, Algeria*

**ARTICLE INFO**

**Article Type:**

**Research Article**

**Received:2025.10.18**
**Accepted in revised form:2025.12.08**

**Keywords**:
Renewable energy;
Solar chimney;
Turbine;
Design;
CFD

**A B S T R A C T**

This study examines the performance improvement of Solar Chimneys Power Plants (SCPPs) through optimized turbine design using three-dimensional numerical simulation. The research contributes to ongoing efforts to advance clean and advanced renewable-energy systems intended to limit reliance on traditional fossil fuels. A simplified 3D computational model of an SCPP, based on the Manzanares prototype, was developed and analyzed in ANSYS Fluent to evaluate three radial turbine configurations. The designs incorporate exit angles of 72.5°, 75°, and 78.5°, coupled with appropriate blade numbers of 12, 14, and 16, respectively. The numerical results reveal that the 14-blade configuration (Design B) achieves the highest performance, generating 70.6 kW of power representing a 43.9% improvement over the reference Manzanares model (49.06 kW), while maintaining stable airflow and thermodynamic characteristics. The obtained results emphasize the critical role of turbine geometry on SCPP efficiency and further demonstrate the system's potential as a reliable and sustainable renewable energy solution, particularly for regions with strong solar resources.

## 1. Introduction

As global pollution levels rise and fossil fuel resources diminish, the demand for sustainable and renewable energy technologies is increasingly urgent. Among the various solar-based solutions, the Solar Chimney Power Plant (SCPP) has emerged as a promising renewable-energy technology capable of

*Corresponding Author Email: bouzida.youcef@univ-khenchela.dz

**Cite this article:** Bouzida, Y., Chehhat, A., Si-Ameur, M. and Arrif, T. (2025). Computational Analysis of Radial Turbine Design and Performance for Renewable Power Generation in Solar Chimney. Journal of Solar Energy Research, 10(4), 2603-2615. doi: 10.22059/jser.2025.404342.1658

DOI: 10.22059/jser.2025.404342.1658

©The Author(s). Publisher: University of Tehran Press.

delivering clean electricity, utility-scale electricity. SCPPs convert solar radiation into mechanical and electrical energy using a combination of thermal buoyancy and aerodynamic processes [1]. The configuration includes three fundamental elements: a solar collector, a tall vertical chimney, and a mechanical conversion unit, most often a turbine [2]. The air confined between the collector and the ground is heated by solar radiation, which reduces its density and causes it to rise because of the resulting pressure difference. This upward airflow, which is rich in thermal and kinetic energy, moves through the chimney and drives the turbine to generate electricity [3].

Extensive research investigated various geometric and operational parameters to enhance SCPP performance. Notable improvements included modifications to the chimney entrance slope and the introduction of constricted sections, both of which helped increase airflow velocity and turbine pressure drop, resulting in higher electrical output [1]. Design optimizations to the collector, such as variations in diameter, inclination, and ground slope, were also shown to significantly improve system efficiency [1, 4]. Additional enhancements, such as the integration of baffles, were demonstrated to improve heat transfer and airflow distribution [5], while the addition of secondary chimneys further boosted energy production [3]. Hybrid configurations, such as the Hybrid Solar Double-Chimney Power Plant (HSDCPP), were also proposed, producing substantial amounts of electricity and distilled water in arid regions [6].

Experimental and numerical studies continued to validate the technology's viability in diverse climates. For example, Bakri et al. [7] confirmed the robust performance of SCPP prototypes in arid conditions, while Ayadi et al. [8] showed that simple modifications, such as adding obstacles at the collector outlet, could increase power output by up to 14.75%. Mustafa et al. [9] reviewed natural and artificial convective vortices and emphasized their ability to generate mechanical energy through buoyancy effects and pressure gradients. They introduced the Atmospheric Vortex Engine (AVE) as a low-cost alternative to physical solar towers and proposed the Solar Vortex Engine (SVE), which used solar heating to sustain artificial vortices. Their analysis confirmed the SVE's feasibility as an innovative approach for power generation. Aziz and Elsayed [10] numerically analyzed over 40 configurations of chimney and collector geometries, making further advancements. They found that increasing the chimney angle up to 3° could enhance the maximum air velocity by 200%, with other parameters, such as collector height and turbine position, also influencing performance. Cuce et al. [4] explored divergent and convergent chimney geometries using a 3D CFD model based on the Manzanares pilot plant. They found that an area ratio (AR) of 4.1 maximized performance, boosting mass flow rate from 1122.1 kg/s to 1629.1 kg/s and increasing efficiency from 0.29% to 0.83%, thereby raising the power output from 54.3 kW to 168.5 kW. Finally, Caicedo [11] proposed a novel radial inflow turbine tailored for SCPPs. Through CFD simulations, the turbine constructed from low-cost materials was shown to generate 77.7 kW, exceeding the output of the original axial turbine at the Manzanares plant by over 40 kW while it maintained comparable efficiency. This underscored the potential for affordable, high-performance turbine alternatives in solar chimney systems.

Danook et al. [12] performed an extensive three-dimensional CFD analysis of a solar chimney system configured according to the Manzanares prototype, integrated with an axial turbine and adapted to the climatic conditions of Kirkuk, Iraq. The study utilized advanced turbulence and radiation models, including the RNG k-ε and non-grey DO radiation models, along with a solar ray tracing algorithm, to evaluate the system's seasonal performance. Results revealed significant variations in air velocity and energy output throughout the year, with July recording the highest air velocity (18.28 m/s) and energy production (14,424 kWh/month) due to elevated ambient temperatures. The normalized daily and monthly electricity production for Kirkuk [12] model reached 310 kWh/day and 9314 kWh/month, respectively, which outperformed the Kubang system and demonstrated the system's viability in similar hot and dry regions. Similarly, Kaplan [13] examined how changes in the inclination angle at the chimney inlet influenced the performance of a Solar Chimney Power Plant (SCPP) using a validated 3D CFD model of the Manzanares prototype. The study explored entrance angles ranging from 50° to 80° while keeping other geometrical parameters constant. The results showed increasing the angle to 80° significantly improved performance metrics, yielding a maximum velocity of 18.1 m/s and a power output of 61.5 kW, representing a 24.5% improvement compared to the base case with a 45° slope. These findings highlighted the significance of chimney entrance geometry in enhancing airflow and energy conversion efficiency in solar chimney systems. Ambient temperature, system dimensions, and solar radiation influenced the performance of SCPPs.

Studies demonstrated that airflow in solar chimney systems peaked around midday, with solar radiation directly influenced power output, though it did not affect chimney efficiency. The best performance was observed in regions with high solar irradiance and lower temperatures, and both system size and solar radiation contributed to increased power output [14]. Geometric modifications, such as reshaping the chimney to a parabolic form, were also found to enhance airflow velocity and overall efficiency [15]. Additionally, the introduction of an annular tower design mitigated boundary layer separation, resulting in a 32% increase in power output [16]. Furthermore, incorporating solar chimneys into desalination systems resulted in a 30% improvement in water production efficiency, particularly under optimal conditions, such as shallow water depths and moderate salt concentrations [17].

Recent studies on Solar Chimney Power Plants (SCPP) highlighted several key improvements in performance. A novel double-pass counter-flow collector design increased efficiency by 28% [18]. Optimizing collector geometry with a convergent outlet also enhanced power generation [19]. In southwestern Iran, sloped SCPPs showed potential to generate 2.98 to 5.91 MW of power [20], while CFD simulations revealed that adjusting geometric parameters and thermal conditions could further improve efficiency and power output [21].

Recent advancements in Solar Chimney Power Plants (SCPP) focused on optimizing various parameters to improve power generation and efficiency. Previous studies demonstrated that modifying key geometric parameters such as modifications to the collector inlet height, chimney diameter, and chimney divergence resulted in substantial improvements in SCPP performance. For example, reducing the collector-inlet height or increasing the chimney diameter was shown to enhance both power output and overall efficiency, with some configurations leading to power generation improvements of up to 12 times the original designs Mandal et al. [22]. Comparative turbine design studies also highlighted that modified blade element theory (BET) based turbines provided the highest power output, indicating the importance of efficient turbine design [23]. Furthermore, comprehensive computational fluid dynamics (CFD) models validated these optimization strategies by accurately simulating airflow and power generation and reinforced the potential of solar chimneys to deliver clean energy in sunny regions. Despite these technological improvements, challenges remained in achieving commercial scalability, requiring further research to optimize plant designs and hybrid systems for real-world applications [24].

The importance of research in Solar Chimney Power Plants (SCPP) lay in its potential to provide a sustainable and eco-friendly energy solution. With the rising demand for renewable energy resources and the imperative to lessen reliance on fossil fuels, SCPPs offered a promising alternative by harnessing solar energy for power generation. The primary driving force behind this research was the need to optimize the design and operational efficiency of SCPPs, thereby enhancing their power output and economic feasibility [25-28].

Recent comprehensive reviews and advanced simulations [29-31] emphasized the significance of geometric optimization, collector material selection, and thermal management in improving system performance. Moreover, hybrid system assessments that integrate solar and biomass sources [32] , as well as advanced CFD-based optimization of semi-elliptical collector geometries [33], provided valuable insights into future directions for SCPP development.

Despite this progress, a significant research gap remains concerning turbine design optimization for SCPPs. Most previous studies have focused on chimney geometry, collector configuration, or environmental effects, while radial turbine performance, blade geometry, and exit angle optimization have received comparatively limited attention, despite their strong influence on energy conversion efficiency. Existing turbine analyses often rely on simplified assumptions, lack detailed fluid–structure interaction considerations, or do not provide comparative evaluations of multiple turbine configurations under identical operating conditions.

The motivation for the present research lay in addressing the need for more efficient and economically viable SCPP systems by improving the performance of the turbine, the central mechanical component that directly determines power output. The novelty of this study rests in its three-dimensional CFD-based investigation of multiple radial turbine configurations with varying exit angles and blade numbers, evaluated under consistent boundary conditions based on the Manzanares prototype. By analyzing airflow patterns, thermodynamic behavior, and power generation characteristics across these designs, the study provides a systematic and comparative assessment of turbine geometry effects.

The aim of this research is to fill the existing gap between theoretical turbine models and practical aerodynamic performance in SCPPs. The findings are

intended to contribute to the development of optimized turbine designs that can improve overall system output, support commercial scalability, and strengthen the role of SCPPs as viable, renewable energy solutions in regions with abundant solar resources.

## 2. Methodology

This study employed a computational simulation–based methodology to examine the performance characteristics of the solar chimney system and to design an optimized radial turbine. The research was conducted in two main phases: the first phase involved simulating the solar chimney without a turbine to establish baseline flow characteristics, while the second phase focused on designing and simulating three radial turbines with different flow angles (72.5°, 75°, and 78.5°), each featuring distinct inlet angles for assessment.

### 2.1. Governing Equations

The transport processes of fluid flow and heat transfer in a solar chimney power plant are described by the conservation equations of mass, momentum, and energy. The corresponding governing equations for this system are as follows [12, 34]:

- Continuity equation:

$$\nabla \cdot \left(\rho \bar{v}\right) = 0 \tag{1}$$

- Momentum equation:

$$\nabla \cdot \left(\rho . v . \vec{v}\right) = -\nabla p + \mu \left[\left(\nabla \vec{v}\right) + \left(\nabla \vec{v}\right)^{T}\right] - \frac{2}{3}\nabla \cdot \vec{v} I + \rho \vec{g} \tag{2}$$

- Energy equation:

$$\nabla \cdot \left(\vec{v}(\rho E + p)\right) = \nabla \cdot \left(k_{eff} \nabla T - h\vec{j} + \left(\mu \left[\left(\nabla \vec{v} + \nabla \vec{v}^{T}\right) - \frac{2}{3}\nabla \cdot \vec{v} I\right]\right), \vec{v}\right) \tag{3}$$

- k-ε equations:

Equation of turbulent kinetic energy, k

$$\frac{\partial}{\partial x_i}\left(\rho k u_i\right) = \frac{\partial}{\partial x_i}\left[\left(\mu + \frac{\mu_t}{\sigma_k}\right)\frac{\partial k}{\partial x_j}\right] + G_k + G_b - \rho \varepsilon Y_M \tag{4}$$

Equation dissipation rate of turbulent kinetic energy, ε

$$\frac{\partial}{\partial x_i}\left(\rho \varepsilon u_i\right) = \frac{\partial}{\partial x_i}\left[\left(\mu + \frac{\mu_t}{\sigma_\varepsilon}\right)\frac{\partial \varepsilon}{\partial x_j}\right] + C_{1\varepsilon}\frac{\varepsilon}{k}\left(G_k + C_{3\varepsilon}G_b\right) - C_{2\varepsilon}\rho\frac{\varepsilon^2}{k} \tag{5}$$

The five empirical constants of k-ε model are typically set as in table 1.

Table 1. The conventional k-ε model coefficients adopted for the present simulations [12]

| $C_{1\varepsilon}$ | $C_{2\varepsilon}$ | $C_{3\varepsilon}$ | $\delta_k$ | $\delta_\varepsilon$ |
|---|---|---|---|---|
| 1.44 | 1.92 | 0.09 | 1.0 | 1.3 |

- Momentum equation of turbine rotation:

The MRF approach approximates rotor motion by solving the flow in a rotating frame around the turbine while maintaining stationary frames elsewhere, providing computational efficiency while capturing key turbine-flow interactions, the equations shall be rearranged as[35]:

$$\nabla \cdot \left(UU\right) = -\frac{1}{\rho}\nabla P + \nabla \cdot \left(\nu \nabla U\right) + \nabla \cdot R \tag{6}$$

The relative velocity and the absolute velocity are related by the eq. (7) as follows:

$$U_r = U - \left(\Omega \times r\right) \tag{7}$$

- The output power of the turbine is given by the following equation [16]:

$$P_t = \frac{2\pi N}{60} \times M \tag{8}$$

### 2.2. Simulation without turbine

This phase focuses on analysing the fundamental airflow characteristics within the solar chimney power plant (SCPP) system prior to the integration of the turbine, using ANSYS Fluent.

#### 2.2.1. Computational Model, Boundary Conditions, and Grid Independence

The numerical model was derived from the architectural configuration of the Manzanares Solar Chimney Power Plant, as depicted in Figure 1, which serves as a widely accepted benchmark for numerical and experimental validation. The prototype features a large circular collector with a gradually rising height profile, the details are presented in table 2[36]. These well-documented dimensions provide a reliable reference for defining the simulation domain, applying appropriate boundary conditions as illustrated in table 4, and ensuring consistency in grid independence assessments as presented in table 5.

Table 2. Main geometric specifications of the Manzanares SCPP [36]

| Parameter | Measurement (m) |
|---|---|
| Mean radius of collector | 122 |
| Mean height of collector | 1.85 |
| Height of chimney | 194.6 |
| Radius of chimney | 5.08 |

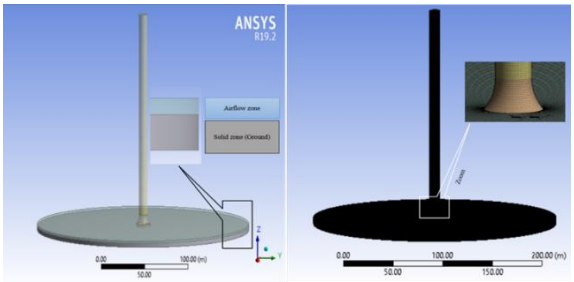


Figure 1. model and mesh of geometry

The collector is semi-transparent, allowing sunlight to penetrate and heat the ground surface. Typically, transparent glass is utilized as the collector material. The materials and physical properties used in the system are detailed in table 3, derived from the pilot facility [25].

Table 3. Material properties applied in the numerical simulations [25]

| Property (unit) | Ground | Aluminium | Glass |
|---|---|---|---|
| Density ($kg/m^3$) | 2160 | 2719 | 2500 |
| Specific heat (J/kg.k) | 710 | 871 | 750 |
| Thermal conductivity (W/m.k) | 1.83 | 202.4 | 1.15 |
| Absorption coefficient | 0.9 | 0 | 0.03 |
| Thickness (m) | 0.5 | 0.00125 | 0.004 |

Table 4. Conditions applied at the simulation boundaries [12]

| Location | Type | Value |
|---|---|---|
| Collector entrance | Pressure inlet | $P_{gage}$ = 0 Pa, Ta = 293.15 K |
| Collector roof | Wall (Glass) | h = 10 W/($m^2$.K) Ta = 293.15K solar irradiation of 1000 W/$m^2$ |
| Ground | Wall | Adiabatic |
| Chimney Wall | Wall | Adiabatic |
| Chimney outlet | Pressure outlet | $P_{gage}$ = 0 Pa |

The model employed the Discrete Ordinates (DO) method in conjunction with a solar ray tracing algorithm. The solar beam direction is input into the program based on the geographical coordinates of the Manzanares which is located at latitude 39 and longitude 3.37 (GMT +2), Spain pilot plant. The geometric dimensions of the system were taken according to the pilot plant [36].

A finite volume framework was adopted to numerically evaluate fluid flow by solving the Navier–Stokes equations together with the governing mass and energy balance equations, The simulations were carried out in ANSYS Fluent (Ansys, Inc., Pennsylvania, USA). The pressure–velocity interaction was solved using the COUPLED algorithm, while turbulence effects were modeled with the RNG k–ε formulation. All governing equations were discretized using second-order upwind schemes for enhanced accuracy. The Boussinesq approximation is applied to account for air density variations due to temperature changes. To ensure precision, double precision was employed for all numerical computations. Convergence criteria are set at $10^{-6}$ for energy and radiation equations and $10^{-4}$ for all other parameters.

Table 5. Grid convergence assessment results for the CFD model

| Cell number | $V_m$ | $\dot{m}$ | % change in $V_m$ | % change in $\dot{m}$ |
|---|---|---|---|---|
| 1286335 | 14.20 | 1060 | — | — |
| 2065689 | 13.14 | 1076 | 5.63 | 1.5 |
| 2763217 | 13.56 | 1083 | 3.13 | 0.65 |

### 2.2.2. Model validation

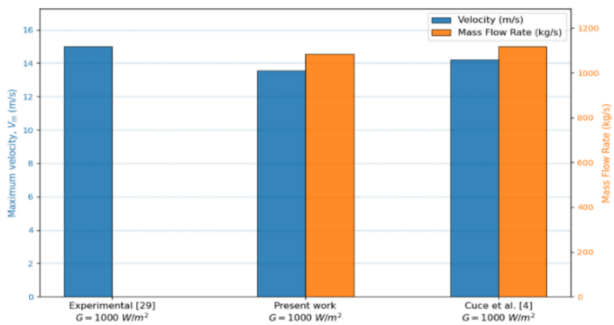


Figure 2. SCPP model validation: Maximum velocity and mass flow rate versus experimental and numerical data

The simulation outcomes were assessed by comparing the computed maximum updraft velocity and mass flow rate with corresponding experimental

data from the Manzanares facility (Haaf 1984) [36] and computational results from Cuce et al. [4]. The simulation was conducted under standard conditions of 1000 W/m² solar radiation.

Table 6. Comparison of present simulation results with experimental and numerical literature

| | Experimental [36] | Our Simulation | Difference (%) | Numerical [4] |
|---|---|---|---|---|
| Updraft Velocity | 15 m/s | 13.56 m/s | 4.5% lower than [4]<br>9.1% lower than [4] | 14.20 m/s |
| Mass flow rate | - | 1083 kg/s | 3.1% lower than [4] | 1117.9 kg/s |

The comparison of the numerical and experimental results revealed a velocity deviation of 9.1%. Although this percentage may appear relatively high, it is mainly attributed to the small reference velocity (15 m/s), where even minor absolute variations result in amplified relative errors. In absolute terms, the deviation corresponds to approximately 1.44 m/s, which remains acceptable for solar chimney flow simulations. Grid independence tests confirmed that further mesh refinement produced negligible changes in the predicted velocity and mass flow rate, ensuring numerical stability. Considering the experimental uncertainty associated with the reference measurements, both the velocity deviation (5–10%) and the mass flow rate deviation (3.1%) fall within the commonly accepted thresholds for CFD validation (5–10%). This consistency demonstrates the robustness and reliability of the numerical model, supporting its use for accurate solar chimney performance evaluation and subsequent design optimization.

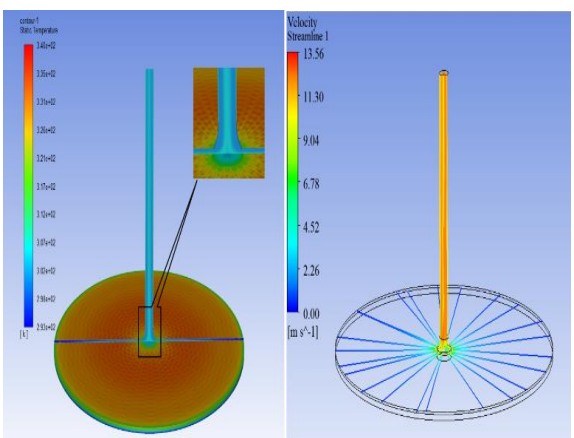


Figure 3. Temperature contours and streamline of air in SCPP model

### 2.3. Turbine design and simulation

The radial inflow turbine was designed using CFturbo computational tools to meet the specified operational requirements of 1083 kg/s mass flow rate at standard ambient temperature conditions (20°C), and the turbine was set to rotate at 14 revolutions per minute (rpm).

Rotor exit diameter ($D_s$) was 10.16 cm. The rotor inlet diameter ($D_1$) was determined using established design principles for radial-inflow turbines. Based on empirical guidelines from [30], the ratio $D_s/D_1$ typically ranges between 0.6 and 0.8, balancing efficiency and compactness. For this study, a rotor inlet diameter ($D_1$) of 15m was selected, corresponding to a ratio of $D_s/D_1 = 0.677$.

Table 7. Main geometric parameters of the turbine

| Main Parameters | Units | Value |
|---|---|---|
| Suction diameter, $d_s$ | (m) | 10.16 |
| Rotor diameter, $d_1$ | (m) | 15 |
| Inlet width, $b_1$ | (m) | 1.85 |
| Blade angle, $\beta_1$ | (°) | 20 |

The number of rotor blades was determined using empirical relations from Glassman's radial turbine design methodology [37]. Based on the stator exit angle (φ1°) and rotor inlet,the blade count formula:

$$n_r = \frac{\pi}{30}(110 - \varphi_1)\tan\varphi_1 \quad (9)$$

This analysis yielded three distinct designs:

Design a (72.5° stator exit angle, 12 blades)
Design b (75° stator exit angle, 14 blades)
Design c (78.5° stator exit angle, 16 blades).

We used CFturbo to verify an acceptable number of stator vanes for the design.

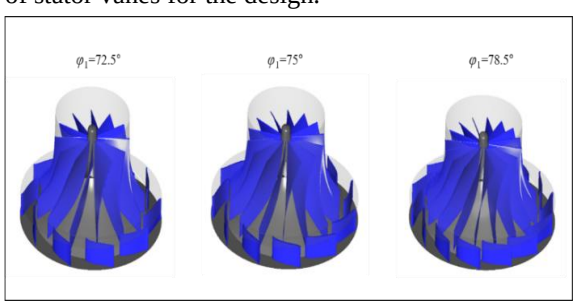


Figure 4. model of three designs in CFturbo

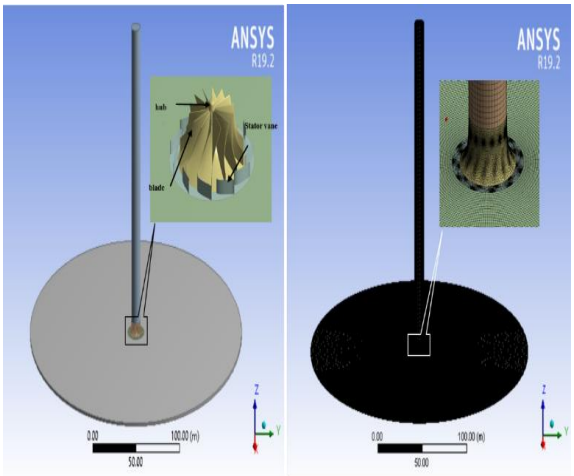


Figure 5. Model and mesh of Manzanares model with radial turbine

Mesh quality is a critical factor in ensuring accurate numerical simulation results. Three distinct mesh configurations were developed to match each design's requirements: the first design used a 2.5 million-cell mesh, the second design employed a 2.6 million-cell mesh, and the third design utilized a 2.7 million-cell mesh. The quality of each mesh was evaluated using skewness and orthogonality, with the first design having skewness 0.15184 and orthogonality 0.85466, the second design having skewness 0.15694 and orthogonality 0.84816, and the third design having skewness 0.16164 and orthogonality 0.84343. These values indicate that the meshes are of good quality, providing adequate resolution of the main flow structures while maintaining computational efficiency across all designs.

For the turbine simulation, we maintained all boundary conditions and solver settings identical to Simulation 1, only introducing the Multiple Reference Frame (MRF) method to model the turbine. The MRF approach approximates rotor motion by solving the flow in a rotating frame around the turbine while maintaining stationary frames elsewhere, providing computational efficiency while capturing key turbine-flow interactions.

## 3. Results and Discussion

The performance characteristics of three radial turbine configurations were evaluated through computational fluid dynamics simulations. This section presents a comparative analysis of airflow velocity profiles, temperature distributions, pressure variations, and power generation capabilities for each design.

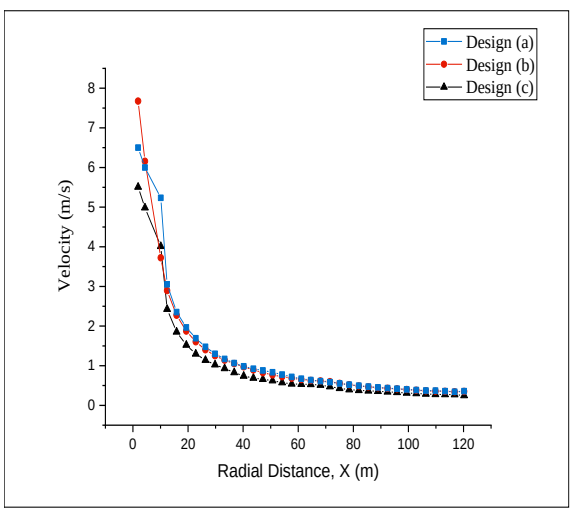


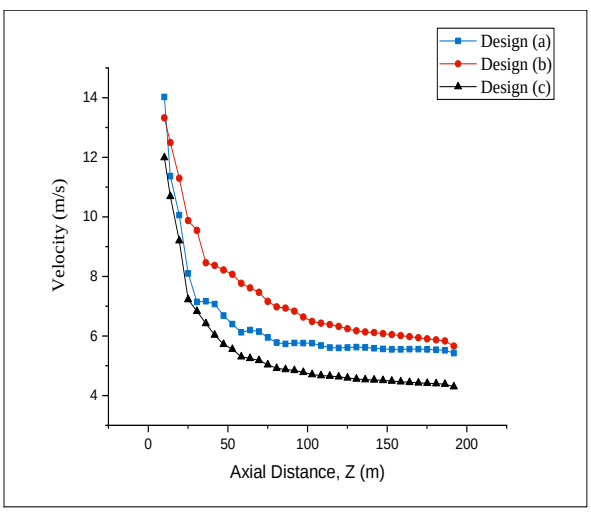


Figure 6. Combined velocity profiles: radial velocity plotted along the X-direction (m) and axial velocity plotted along the Z-direction (m)

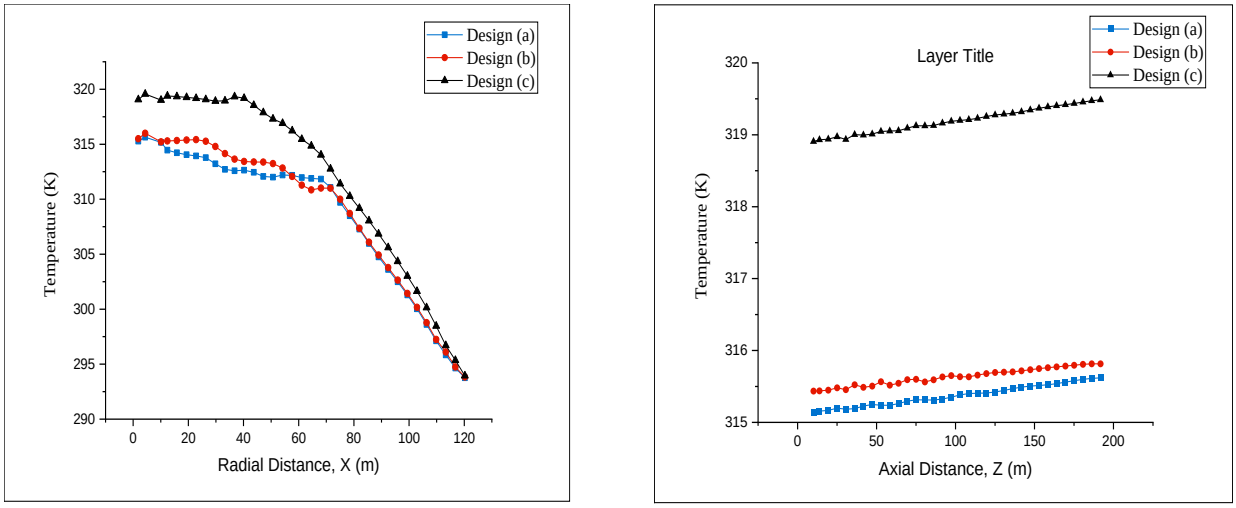


Figure 7. Combined temperature profiles: radial temperature plotted along the X-direction (m) and axial temperature plotted along the Z-direction (m)

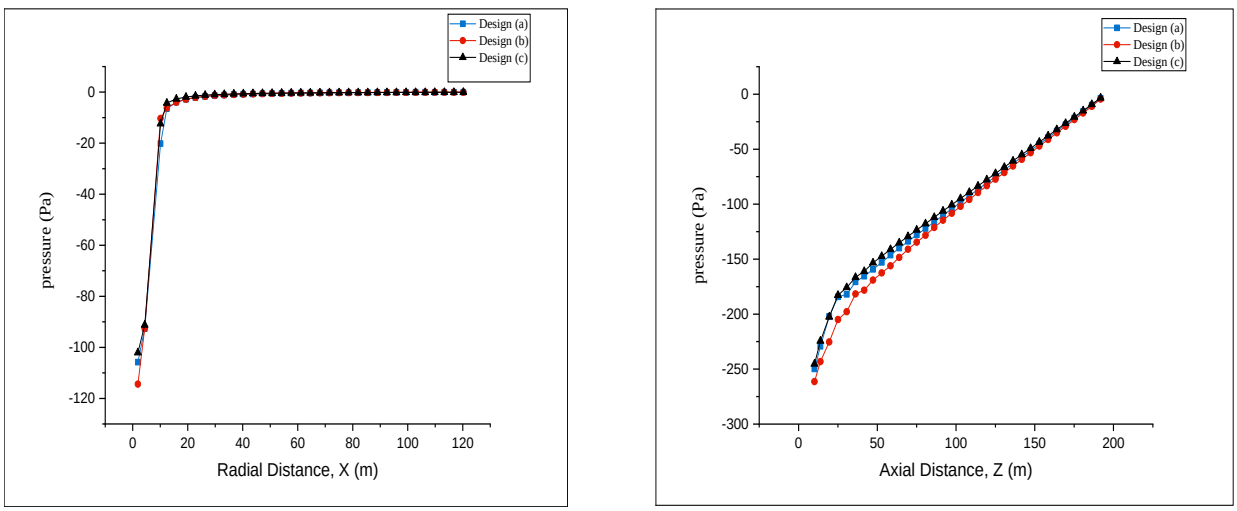


Figure 8. Combined pressure profiles: radial pressure plotted along the X-direction (m) and axial pressure plotted along the Z-direction (m)

The numerical results obtained from the simulations presented in Figures 6 indicate that air velocity within the solar collector and chimney varies markedly depending on the proposed geometric configurations (a, b, and c). The velocity profiles along the collector (X-direction) reveal a gradual decline as the airflow advances towards the center of the collector. This reduction is primarily due to the diminishing thermal driving force and increased frictional losses. Among the designs, Design (b) recorded the highest initial velocity at the collector inlet, suggesting superior performance in accelerating airflow at the entry point, whereas Design (c) demonstrated the weakest performance. In the chimney section (Z-direction), Design (a) exhibited the highest velocities at the base of the chimney, reaching up to 14 m/s, indicating a more effective conversion of thermal energy into kinetic energy through buoyancy-driven flow. Conversely, Design (c) showed considerably lower velocities throughout the chimney, indicating a reduced capacity for transporting and accelerating heated air. The findings emphasize the important role of system geometry in determining the efficiency of a solar chimney, with

Design (a) identified as the most effective configuration within the defined conditions.

The numerical results illustrated in Figure 7 demonstrate the variation in air temperature within the solar chimney system for the three geometric configurations (Designs a, b, and c). The radial temperature distribution as a function of X, (left panel of Figure 7) shows that temperatures generally decrease with increasing distance from the center

towards the edge of the collector. Among the three configurations, Design (c) maintains the highest overall temperatures throughout the collector region, suggesting a more effective retention or absorption of thermal energy, followed by Designs (b) and (a). This indicates that Design (c) likely facilitates better heat accumulation under the transparent roof, possibly due to improved insulation or geometrical features enhancing solar gain.

The axial temperature profile as a function of Z (right panel of Figure 7) reveals that, although the overall temperature difference along the chimney is modest, Design (c) again records the highest temperatures, with a slight but consistent upward trend. This suggests that the heated air in Design (c) retains more thermal energy as it ascends, enhancing buoyancy-driven flow. In contrast, Designs (a) and (b) exhibit lower temperature gradients, which could lead to a reduced buoyancy effect and less efficient thermal-to-kinetic energy conversion.

These findings underscore the importance of temperature management in solar chimney design. While Design (a) performed best in terms of airflow velocity, Design (c) demonstrates superior thermal characteristics, indicating a potential trade-off between thermal retention and flow acceleration. Optimal performance would ideally balance both aspects to maximize overall system efficiency.

The pressure distribution results presented in Figure 8 illustrate the radial and axial pressure variations within the solar chimney system for the three configurations. The radial pressure profile (left side of Figure 8) shows a sharp drop occurs near the center of the collector, followed by a rapid stabilization across all designs. Design (b) exhibits the lowest pressure at the inlet, indicating a stronger suction effect that may enhance airflow induction.

In the axial pressure profile (right side of Figure 8), all designs show a consistent pressure drop with height, characteristic of buoyancy-driven flow. Design (c) maintains slightly higher pressures along the chimney, which may indicate increased flow resistance.

Overall, the pressure profiles reflect the influence of geometry on driving forces and confirm that efficient pressure gradients are essential for sustaining airflow within the system.

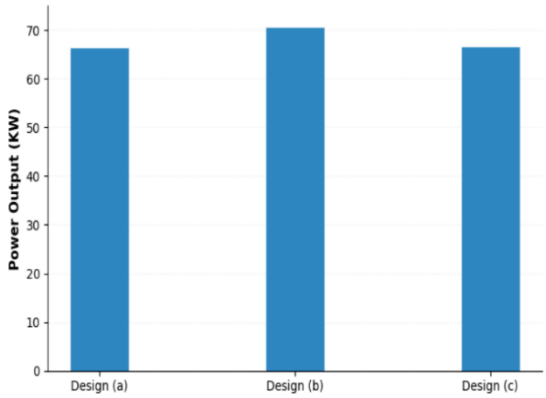


Figure 9. Power output of three designs

Figure 9 illustrates the power output and mass flow characteristics of the three proposed designs. Design (a) produced 66.5 kW of power, accompanied by a mass flow rate of 530 kg/s.. This configuration serves as the baseline, reflecting a design optimized for high fluid throughput with minimal flow resistance. However, the moderate power output suggests limitations in energy conversion efficiency, possibly due to less-than-ideal blade angles or flow separation effects within the rotor geometry.

The torque for the second design (b) is 48.15 kN.m, generating 70.6 kW of power while maintaining a comparable mass flow rate of 520 kg/s. This 6.2% power increase over design a, achieved with only a 1.9% reduction in mass flow, confirms the effectiveness of its 14-blade arrangement, demonstrating superior energy transfer capability while successfully balancing flow capacity with enhanced power conversion, making it particularly suitable for applications requiring maximum performance without significant flow restriction.

Design (c) yields a power output of 66.7 kW, accompanied by a reduced mass flow rate of 455 kg/s, a 14% decrease compared to design (a). This reduction is attributed to the higher blade count and the integration of guide vanes, which, while improving flow control and directionality, introduce greater flow resistance. This design is more specialized, potentially favoring applications where controlled flow and stability are prioritized over maximum throughput.

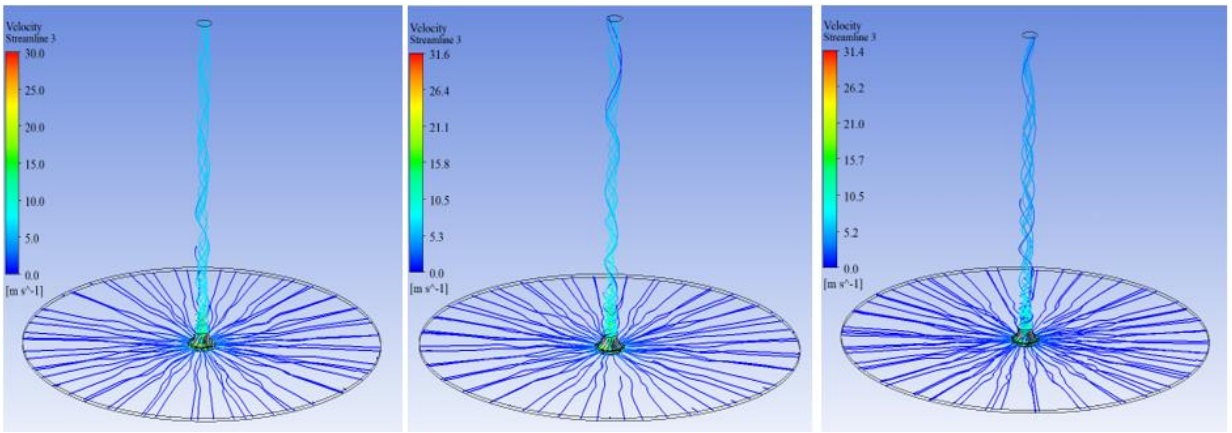


Figure 10. Streamline of air in SCPP model

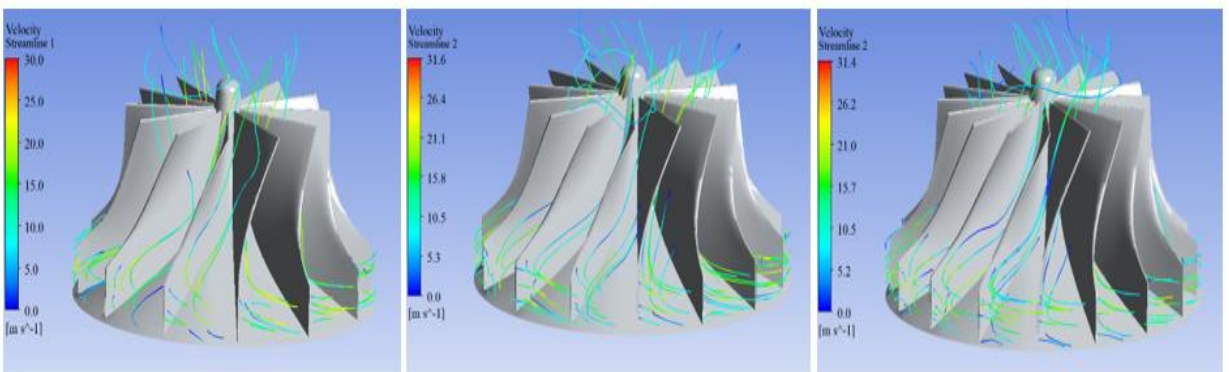


Figure 11. Streamlines through the rotor

Figures 10 and 11 present the streamline visualization of airflow within the Solar Chimney Power Plant (SCPP) model, offering insight into the aerodynamic performance of different rotor designs.

In Figure 10, the streamline plots illustrate the general airflow pattern from the collector region towards and through the chimney. All three configurations show a smooth radial inflow towards the center, followed by a strong vertical acceleration up the chimney. However, differences in streamline density and velocity magnitude indicate varying efficiencies. The middle configuration exhibits the most concentrated and vertically aligned streamlines, suggesting enhanced flow stability and stronger buoyancy-driven uplifts, which are critical for efficient turbine operation. This correlates with its superior power output, seen in earlier results.

Figure 11 focuses on the interaction of airflow with the rotor blades. The streamlines reveal the degree of flow attachment and deflection across different blade designs. In the first configuration, the flow shows mild separation, which can reduce torque generation. The second design demonstrates smoother flow paths around the blades with minimal recirculation, indicating optimal incidence angles and efficient momentum transfer to the rotor. The third design, although featuring guide vanes for flow direction control, shows some local disturbances and flow detachment, likely due to increased aerodynamic resistance from the denser blade arrangement.

## 4. Conclusions

This study performed an extensive CFD analysis of various radial turbine configurations integrated into a Solar Chimney Power Plant (SCPP), focusing on the influence of blade number and exit angle on system performance. The results demonstrate that turbine geometry exerts a decisive impact on energy conversion efficiency, airflow stability, and thermodynamic behavior. Among the three tested designs, the configuration with a 75° exit angle and 14 blades achieved the highest performance, producing 70.6 kW of power, representing a 43.9% improvement over the Manzanares reference model while maintaining stable mass flow and pressure gradients.

Critical analysis revealed that lower blade counts favored higher throughput but limited conversion efficiency, whereas higher blade densities enhanced

thermal retention but introduced excessive flow resistance. The intermediate configuration provided the optimal compromise, confirming the necessity of balancing aerodynamic efficiency with flow stability. Streamline and velocity profile evaluations further highlighted the importance of minimizing recirculation losses and ensuring effective buoyancy-driven uplift.

These findings underscore turbine design as a primary bottleneck in SCPP optimization, a dimension often underexplored compared to chimney or collector geometries. By bridging theoretical turbine models with validated CFD simulations, this work contributes to the advancement of economically viable and scalable SCPP systems. Future research should extend toward fluid–structure interaction, material durability, and hybrid integration strategies to consolidate the role of solar chimney technology as a reliable renewable energy solution in regions with high solar irradiance.

**Nomenclature**

| | |
|---|---|
| CFD | Computational fluid dynamics |
| MRF | Multiple Reference Frame |
| SCPP | Solar Chimney Power Plant |
| $b_1$ | Inlet width of the turbine (m) |
| $C_{1\varepsilon}$, $C_{2\varepsilon}$, $C_{3\varepsilon}$ | Empirical constants of k–ε model (-) |
| $C_P$ | Specific heat capacity at constant pressure (J/kg.K) |
| D | Diameter (m) |
| g | Gravitational acceleration (m/s$^2$) |
| $G_b$ | Turbulent kinetic energy generation due to buoyancy (m$^2$/s$^3$) |
| $G_k$ | Turbulent kinetic energy generation due to mean velocity gradients (m$^2$/s$^3$) |
| h | Heat transfer coefficient (W/m$^2$.K) |
| K | Turbulent kinetic energy (m$^2$/s$^2$) |
| M | Torque (N·m) |
| $\dot{m}$ | Mass flow rate (kg/s) |
| N | Rotational speed (rpm) |
| $n_r$ | Number of rotor blades |
| P | Pressure (Pa) |
| $P_t$ | Turbine power output (kW) |
| r | distance from the cell centroid to the rotation axis |
| R | Reynolds stress tensor |
| T | Temperature (K) |
| t | Time (s) |
| U | absolute velocity (m/s) |
| $U_r$ | the relative velocity (m/s) |
| β | Blade angle (°) |
| ε | Turbulent dissipation rate (m$^2$/s$^3$) |
| μ | Dynamic viscosity (kg/m·s) |
| ρ | Density (kg/m$^3$) |
| Ω | Angular velocity (rad/s) |

**References**


1. Kaplan, M. (2025). The effect of chimney entrance slope and constricted section on the performance of solar chimney power plants: A CFD approach. In *E3S Web of Conferences* (Vol. 601, pp. 00003): EDP Sciences.https://doi.org/10.1051/e3sconf/202560100003.
2. Abdelsalam, E., F. Almomani, H. Alnawafah, D. Habash, and M. Jamjoum. (2024). Sustainable production of green hydrogen, electricity, and desalinated water via a Hybrid Solar Chimney Power Plant (HSCPP) water-splitting process. *International Journal of Hydrogen Energy*, *52*, 1356–1369. https://doi.org/10.1016/j.ijhydene.2023.06.165.
3. Abdelsalam, E., F. Kafiah, F. Almomani, M. Tawalbeh, S. Kiswani, A. Khasawneh, D. Ibrahim, and M. Alkasrawi. (2021). An innovative design of a solar double-chimney power plant for electricity generation. *Energies*, *14*(19), 6235. https://doi.org/10.3390/en14196235.
4. Cuce, E., A. Saxena, P.M. Cuce, H. Sen, S. Guo, and K. Sudhakar. (2021). Performance assessment of solar chimney power plants with the impacts of divergent and convergent chimney geometry. *International Journal of Low-Carbon Technologies*, *16*(3), 704–714. https://doi.org/10.1093/ijlct/ctaa097.
5. Wang, J., J. Nie, J. Jia, H. Su, R. Tian, S. Yan, and H. Gao. (2022). Structural optimization to reduce the environmental crosswind negative influence on the performance of a solar chimney power plant system. *Solar Energy*, *241*, 693–711. https://doi.org/10.1016/j.solener.2022.06.015.

6. Abdelsalam, E., F. Almomani, S. Ibrahim, F. Kafiah, M. Jamjoum, and M. Alkasrawi. (2023). A novel design of a hybrid solar double-chimney power plant for generating electricity and distilled water. *Sustainability*, *15*(3), 2729. https://doi.org/10.3390/su15032729.
7. Badis, B., B. Hani, N. Haythem, and D. Zied. (2023). Experimental Study of Solar Chimney Power Plant. *Journal of Advanced Research in Fluid Mechanics and Thermal Sciences*, *101*(1), 207–214. https://doi.org/10.37934/arfmts.101.1.207214.
8. Ayadi, A., Z. Driss, and M.S. Abid. (2020). The impact of placing obstacles on the distribution of the airflow inside a solar chimney. *Environmental Progress & Sustainable Energy*, *39*(3), e13379. https://doi.org/10.1002/ep.13379.
9. Mustafa, A.T. (2015). A review of convective and artificial vortices for power generation. *International Journal of Sustainable Development and Planning*. https://doi.org/10.2495/sdp-v10-n5-650-665.
10. Aziz, M.A. and A.M. Elsayed. (2022). Thermofluid effects of solar chimney geometry on performance parameters. *Renewable Energy*, *200*, 674–693. https://doi.org/10.1016/j.renene.2022.10.022.
11. Caicedo, P., D. Wood, and C. Johansen. (2021). Radial turbine design for solar chimney power plants. *Energies*, *14*(3), 674. https://doi.org/10.3390/en14030674.
12. Danook, S.H., H.A. AL-bonsrulah, I. Hashim, and D. Veeman. (2021). CFD simulation of a 3D solar chimney integrated with an axial turbine for power generation. *Energies*, *14*(18), 5771. https://doi.org/10.3390/en14185771.
13. Kaplan, M. (2023). Influence of inclination angle at the chimney inlet on the power generation in solar chimney power plants through 3D CFD model. *International Journal of Photoenergy*, *2023*(1), 7394007. https://doi.org/10.1155/2023/7394007.
14. Kasaeian, A.B., M. Amirifard, M.H. Ahmadi, and F. Kasaeian. (2017). Investigation of the effects of ambient temperature and dimensional parameters on the performance of solar chimney power plants. *International Journal of Low-Carbon Technologies*, *12*(4), 335–348. https://doi.org/10.1093/ijlct/ctw016.
15. Jameei, A., P. Akbarzadeh, H. Zolfagharzadeh, and S. Eghbali. (2019). Numerical study of the influence of geometric form of chimney on the performance of a solar updraft tower power plant. *Energy & Environment*, *30*(4), 685–706. https://doi.org/10.1177/0958305x18802908.
16. Kasaeian, A., A.R. Mahmoudi, F.R. Astaraei, and A. Hejab. (2017). 3D simulation of solar chimney power plant considering turbine blades. *Energy Conversion and Management*, *147*, 55–65. https://doi.org/10.1016/j.enconman.2017.05.029.
17. Kebabsa, H., M.S. Lounici, and A. Daimallah. (2021). Numerical investigation of a novel tower solar chimney concept. *Energy*, *214*, 119048. https://doi.org/10.1016/j.energy.2020.119048.
18. Nasraoui, H., Z. Driss, and H. Kchaou. (2020). Novel collector design for enhancing the performance of solar chimney power plant. *Renewable Energy*, *145*, 1658–1671. https://doi.org/10.1016/j.renene.2019.07.062.
19. Ayadi, A., Z. Driss, and M.S. Abid. (2019). Experimental and computational analysis of the collector geometry of a solar chimney. *Environmental Progress & Sustainable Energy*, *38*(6), e13238. https://doi.org/10.1002/ep.13238.
20. Maghrebi, M.J., R. Masoudi Nejad, and S. Masoudi. (2017). Performance analysis of sloped solar chimney power plants in the southwestern region of Iran. *International Journal of Ambient Energy*, *38*(6), 542–549. https://doi.org/10.1080/01430750.2016.1155487.
21. Torabi, M.R., M. Hosseini, O.A. Akbari, H.H. Afrouzi, D. Toghraie, A. Kashani, and A.a. Alizadeh. (2021). Investigation the performance of solar chimney power plant for improving the efficiency and increasing the outlet power of turbines using computational fluid dynamics. *Energy Reports*, *7*, 4555–4565. https://doi.org/10.1016/j.egyr.2021.07.044.
22. Mandal, D.K., N. Biswas, N.K. Manna, D.K. Gayen, and A.C. Benim. (2024). An

application of artificial neural network (ANN) for comparative performance assessment of solar chimney (SC) plant for green energy production. *Scientific Reports*, *14*(1), 979. https://doi.org/10.1038/s41598-023-46505-1.

23. Esmail, M.F.C., W.M. A-Elmagid, T. Mekhail, I.M. Al-Helal, and M.R. Shady. (2021). A numerical comparative study of axial flow turbines for solar chimney power plant. *Case Studies in Thermal Engineering*, *26*, 101046. https://doi.org/10.1016/j.csite.2021.101046.
24. Biswas, N., D.K. Mandal, S. Bose, N.K. Manna, and A.C. Benim. (2023). Experimental Treatment of Solar Chimney Power Plant—A Comprehensive Review. *Energies*, *16*(17). https://doi.org/10.3390/en16176134.
25. Cuce, E., P.M. Cuce, and H. Sen. (2020). A thorough performance assessment of solar chimney power plants: Case study for Manzanares. *Cleaner Engineering and Technology*, *1*, 100026. https://doi.org/10.1016/j.clet.2020.100026.
26. Hasan, M.K., A. Gross, L. Bahrainirad, and H.F. Fasel. (2022). Investigation of collector flow for 1:30 scale solar chimney power plant model. *Solar Energy*, *241*, 220–230. https://doi.org/10.1016/j.solener.2022.05.059.
27. Ganguli, A.A., S.S. Deshpande, and A.B. Pandit. (2021). CFD Simulations for Performance Enhancement of a Solar Chimney Power Plant (SCPP) and Techno-Economic Feasibility for a 5 MW SCPP in an Indian Context. *Energies*, *14*(11). https://doi.org/10.3390/en14113342.
28. Buckland, G. and J. Booker. (2025). Scaled Designs of Solar Chimneys for Different Locations. *Designs*, *9*(1). https://doi.org/10.3390/designs9010001.
29. Araya, H.G. and S.T. Teferi. (2025). Performance Comparison of Cylindrical and Diverging Solar Chimney Power Plants. *Results in Engineering*, 105485. https://doi.org/10.1016/j.rineng.2025.105485.
30. Hashemian, N. and A. Noorpoor. (2023). Thermo-eco-environmental investigation of a newly developed solar/wind powered multi-generation plant with hydrogen and ammonia production options. *Journal of Solar Energy Research*, *8*(4), 1728–1737. https://doi.org/10.22059/jser.2024.374028.1388.
31. Benettayeb, Y., A. Benbouali, T. Tahri, and E. Cuce. (2025). Performance analysis of the impact of sloped absorber dimensions on the performance of solar chimney power plants. *Journal of Thermal Analysis and Calorimetry*, *150*(12), 9561–9571. https://doi.org/10.1007/s10973-025-14307-4.
32. Hashemian, N. and A. Noorpoor. (2019). Assessment and multi-criteria optimization of a solar and biomass-based multi-generation system: Thermodynamic, exergoeconomic and exergoenvironmental aspects. *Energy Conversion and Management*, *195*, 788–797. https://doi.org/10.1016/j.enconman.2019.05.039.
33. Natarajan, R., S. Yaknesh, K.B. Prakash, M. Al Awadh, and Q.M. Al-Mdallal. (2025). Parametric optimization of flow in a solar chimney power plant under variable semi elliptical constraints. *Scientific Reports*, *15*(1), 331. https://doi.org/10.1038/s41598-024-82953-z.
34. Cuce, P.M., E. Cuce, S. Alshahrani, S. Saboor, H. Sen, I. Veza, and C.A. Saleel. (2022). Performance Evaluation of Solar Chimney Power Plants with Bayburt Stone and Basalt on the Ground as Natural Energy Storage Material. *Sustainability*, *14*(17), 10960. https://doi.org/10.3390/su141710960.
35. Reid, A., R. Rossi, C. Cottini, and A. Benassi. (2025). CFD simulation of a Rushton turbine stirred-tank using open-source software with critical evaluation of MRF-based rotation modeling. *Meccanica*, *60*(6), 1613–1637. https://doi.org/10.1007/s11012-024-01824-z.
36. Haaf, W. (1984). Solar Chimneys. *International Journal of Solar Energy*, *2*(2), 141–161. https://doi.org/10.1080/01425918408909921.
37. Glassman, A.J. (1976). *Computer program for design analysis of radial-inflow turbines* (NASA-TN-D-8164).